Title

Variations in turbulent energy dissipation and water column stratification at the entrance of a tidally energetic strait

Authors

Shiho Kobayashi[1]*, Eisuke Hashimoto[2], Masayuki Nagao[3], Yoshio Takasugi[2]

*corresponding author
e-mail address: shihok@kais.kyoto-u.ac.jp
tel: +81-75-753-6216

[1] Graduate School of Agriculture, Kyoto University, Kitashirakawaoiwake, Sakyo, Kyoto, 606-8502, Japan

[2] National Institute of Advanced Industrial Science and Technology (AIST Chugoku), 2-2-2, Hiro, Kure, Hiroshima, 737-0197,Japan

[3] National Institute of Advanced Industrial Science and Technology (AIST Tsukuba), 1-1-1, Tsukuba-Higashi, Ibaragi, 305-8567,Japan

Abstract

We observed tidal currents, turbulent energy dissipation and water column stratification at the entrance of a narrow strait (Neko Seto) in the Seto Inland Sea, Japan, using a free-falling turbulence micro-structure profiler (TurboMap) and Acoustic Doppler Current Profiler (ADCP). The variation in turbulent energy dissipation at the entrance of the strait was not at quarter-diurnal frequency but at semi-diurnal frequency; turbulent energy dissipation was enhanced during the ebb tide, although it was moderate during the flood tide. This result is consistent with the results of Takasugi (1993), which showed the asymmetry of tidal energy loss during a semi-diurnal tidal cycle using control volume analysis. It is suggested that significant turbulent energy dissipation is generated in the strait, which influences the properties of water outside the strait when tidal currents flow out from the strait.

Running Title

turbulent energy dissipation at the entrance of a tidally energetic strait

Keywords

tidal currents; turbulent energy dissipation; tidal variation; tidally energetic strait; Seto Inland Sea

和文タイトル

潮流の強い海峡部開口部付近における乱流エネルギー逸散および水柱構造の変動

日本語著者名

小林志保・橋本英資・長尾正之・高杉由夫

日本語要旨

自由落下式乱流微細構造プロファイラ (TurboMap) 及び 超音波ドップラー流速計 (ADCP)を用いて瀬戸内海の海峡部（猫瀬戸）入口において潮流，乱流エネルギー逸散率及び物理構造の観測を行なった．猫瀬戸入口における乱流エネルギー逸散率は M_4 周期ではなく M_2 周期で変化していた．下げ潮流時には乱流エネルギー逸散率が増大するが，上げ潮流の増大は比較的穏やかであった．この結果は，コントロールボリューム法を用いて潮汐エネルギーの損失が上げ潮流時と下げ潮流時とで異なることを示した高杉 (1993) の結果と一致している．下げ潮流時には海峡内において大きな乱流エネルギー逸散が生じ，さらに海峡外の水の性質に大きな影響を及ぼすことが示唆された．

1. Introduction

The Seto Inland Sea is a semi-enclosed coastal sea connected to the Pacific Ocean through two openings separated by an along-channel distance of ~ 550 km. It resembles an archipelago due to the presences of hundreds of islands and a number of narrow straits where strong tidal currents generate vigorous stirring. The spatial pattern of varying stratification is reflected to a considerable degree in the distributions of biochemical properties in the Seto Inland Sea; in most straits, vertical differences in nutrients and chlorophyll are small or negligible, while, in the stagnant basins, there are pronounced vertical differences associated with density stratification (Kobayashi et al., 2006). Turbulent mixing may play an important role in controlling the water column stratification.

The tidal cycle of turbulent energy dissipation has been studied previously in coastal and shelf seas (e.g., Simpson et al., 2002; Inall et al., 2004; Souza et al., 2008). Rippeth et al. (2003) illustrated the tidal cycle of turbulent energy dissipation in an energetic tidal flow, while Matsuno and Nakata (2004) showed this in Ariake Bay, Japan. Although the interaction between tidal currents and turbulent energy dissipation in these shelf seas or bays has been demonstrated, few studies have been conducted on turbulence measurements in the straits in archipelagos.

Yamazaki et al. (2006) first provided microstructural data in a tidally energetic strait in the Seto Inland Sea (Neko Seto, 34°10’N, 132°30’E) obtained from a turbulent micro-structure profiler (TurboMAP, Wolk et al., 2002). Mitchell et al. (2008) also published the results of observations in the Neko Seto, with microscale profiles with considerable structure, particularly shear. The tidal cycle in turbulent microstructures in such straits has not been fully elucidated.

This study presents a tidal cycle of turbulent microstructure obtained from TurboMAP at the entrance of Neko Seto, a tidally energetic strait in the Seto Inland Sea. We first demonstrate the temporal variations in turbulent energy dissipation, temperature and conductivity measured using TurboMAP. The temporal variation in tidal energy dissipation is interpreted on the basis of flow fields measured using an Acoustic Doppler Current Profiler (ADCP).

2. Study Area

The study area is located at the entrance of the narrow strait Neko Seto in the Seto Inland Sea (Fig. 1b). The width of the narrowest part of the strait is about 1.5 km, with the width increasing exponentially at the strait's entrance. The topography of the study area is complicated, with depth varying from 10 to 110 m (Fig. 1c). Takasugi (1993) described the distribution of the amplitude of the M_2 tidal current in Neko Seto obtained from long-term mooring of a current meter. The amplitude at the narrowest part exceeds 1.5 m s^{-1}, while far from the narrowest part it is around 0.1 m s^{-1}. As with all straits in the Seto Inland Sea, the narrowest part in Neko Seto, where the amplitude of the tidal current is largest, is the deepest. This is attributed to the intensified tidal currents eroding the seabed (Takeoka, 2002).

Maximum ebb and flood currents in this region appear around 2 hours before low and high water, respectively (Takasugi, 1987). When tidal currents pass through the strait, tidal jets accompanied by significant horizontal shear are formed at the entrance. Takasugi et al. (1989) described the sheared flow according to ADCP measurement, finding significant tidal energy loss within the sheared flow. Tidal vortexes are also formed in this region, similar to those at the entrances of Akashi and Naruto Straits (Takasugi, 1987). The topography and tidal currents in the study area are thus extremely complicated.

Takasugi (1993) revealed the tidal energy balance in the study area, based on the results of the current measurements at the stations indicated by circles in Fig. 1c (C1~C6) and sea level measurements at four points around the strait (details of the analysis are shown in the Appendix). Fig. 2 shows the temporal variations in each term, estimated using control volume analysis. He found that the energy loss, E_f, reaches 2.5 × 10^4 W m^{-1} (~ 0.5 W m^{-3} when divided by the sectional area) during maximum ebb. He also found that the magnitude of E_f changes according to the current direction; it became larger in westward (ebb tide) than that in eastward flow (flood tide).

3. Methods

3-1. Observation Program and Meteorological Condition

Observations were made on 6 July, 2005, from 07:30 to 20:30 h, JST, covering a complete M_2 tidal cycle. It was cloudy and the weather was calm on the observation date. Daily mean wind speed obtained by the Japan Meteorological Agency at a weather station in Kure (the location of Kure is shown in Fig. 1b) was 1.5 m s^{-1} and hourly changes in wind speed were insignificant.

The locations of the stations are shown in Fig. 3. The ship ran between stations 1 to 4 during the observation period, stopping at each station for 5 minutes to measure currents and turbulent microstructures according to the methods described below. A total of 14 measurements were taken at each station during the observation period.

3-2. Flow Fields and Velocity Shear

Bottom-track velocities were obtained for a period of 5 minutes at 2-second intervals at each station using a ship-mounted Acoustic Doppler Current Profiler (ADCP) (R. D. Instruments) operating at 600 kHz through four beam transducers directed 20 degrees from the vertical. The first ADCP measurement bin was set immediately below the blanking interval (3.1 m depth), and subsequent bins sampled down to the bottom at 2 m intervals in bottom track mode. Velocities could not be obtained at the bottom and in the surface 10% of the water depth. Data at station 4 at 15:50 h were obtained only in the upper 30 m, for reasons unknown.

The data obtained from ADCP were corrected using pitch and roll data provided by a tiltmeter. Velocity data in which Percent Good value of beam velocity was less than 80% were removed. The remaining data were averaged to obtain the profile at each station for each cycle.

The squared velocity shear (S^2) was then calculated at 2 m intervals using the following equation:

$$S^2 = \left(\frac{\partial u}{\partial z}\right)^2 + \left(\frac{\partial v}{\partial z}\right)^2 \quad ,$$

where z is the vertical coordinate and u and v are the eastward and northward components of velocity, respectively. These values were interpolated into 1 m interval data.

3-3. Turbulent Microstructure

The vertical profiles of turbulent microstructure were measured using a Turbulent Ocean Microstructure Acquisition Profiler (TurboMAP) (Wolk et al., 2002). The instrument used was a free-falling profiler that carries microstructure sensors, Conductivity-Temperature-Depth (CTD) sensors, and internally mounted accelerometers. The buoyancy of the instrument was adjusted to provide a free-fall sinking velocity of 0.7 m s^{-1}, and the signals were sampled at 512 Hz. Data were used from the depth range in which the time-rate-change of the sinking velocities was less than 0.035 m s^{-1} (the mechanical error of sinking velocity; ~5 %; Oakey and Elliott, 1970). To avoid data contamination due to initial perturbation of the instrument, data in the surface layer (~ 4 m) were removed.

We dropped the TurboMAP after waves and visible bubbles generated by the screw of the ship had dissipated and pulled it up after the instrument reached the bottom. Shear data in the bottom 30 cm could not be obtained because of the shear probe protector. Data below 90 m at station 4 were not obtained when the tidal current was strongest (at 14:10 h and 14:50 h, JST), because significant upward velocities prevented the instrument from sinking.

Shear data were processed using the software tmTooLs, which uses a variable integration method to avoid mechanical vibrations and electronic noise. To compute the turbulent kinetic energy dissipation rate (ε), power spectra were obtained from the observed shear data by Fourier transform every 512 points (overlap 256 points). The spectra were corrected by the method of Oakey (1982). The spectra were then integrated over an appropriate wave number band. The range of integration was determined on the basis of fitting the Universal Spectrum (Nasmyth, 1970) to the observed spectrum.

4. Results

Fig. 4 shows the temporal variations in tidal height on 6 July 2005 (from 08:00 to 20:00 h, JST) predicted using tidal constituents (M_2, S_2, K_1, O_1) provided by the Maritime Safety Agency, Japan. The first high water was identified at 09:00 h; ebb tide started thereafter. Low water was found at 15:00 h; the flood tide then started and the subsequent high water appeared around 21:30 h.

A semi-diurnal variation in water column stratification was observed in the study area; axial sections of water temperature, salinity and density in the upper layer (0 ~ 40 m) around 09:00 h (high water), 13:00 h (ebb tide), 15:00 h (low water) and 18:00 h (flood tide) are shown in Fig. 5. A source of low-salinity, warm water existed around the station farthest from the strait (Sta. 1). At high water (Fig. 5 a ~ c), the low-salinity, warm water spread over the layer above 10 m, reaching the station closest to the strait (Sta. 4). Both temperature and salinity in the layer below 10 m were almost uniform throughout the study area. Density was also almost uniform in the layer below 10 m, with only one isopycnal tilted upward toward the strait.

During ebb tide (Fig. 5 d ~ f), the low-salinity, warm water was pushed back toward Sta. 1. The thermocline, halocline and pycnocline in the surface layer were unstrained, and part of surface warm water was mixed with water in the lower layer at Sta. 4. A high-salinity water mass (32.8 psu) was found around the bottom of Stas. 2 and 3. Density was still almost uniform in the layer below 5 m, with only one isopycnal tilted downward toward the strait. At low water (Fig. 5 g ~ i), the low-salinity, warm water was found only at Sta. 1, and the thermocline, halocline and pycnocline were intensified and moved up to the near-surface. A high-salinity water mass (32.8 psu) left the strait and was found on the bottom of Sta. 1. During flood tide (Fig. 5 j ~ l), the low-salinity, warm water began to spread toward the strait.

Fig. 6 shows semi-diurnal variations in the eastward and northward components of velocity (m s^{-1}) measured using ADCP. The data show that the tidal currents in this region generally flow to the northeast during the flood and to the southwest during the ebb tide. At the stations far from the strait (Stas. 1 and 2), the direction of the currents changed from the northeast to the southwest at high water, and from the southwest to the northeast at low water. At the stations near the strait (Stas. 3 and 4), the currents show considerable irregularity during ebb tide; they were directed to the northeast at high water but turned to the southwest thereafter, then returned to the northeast. Vertical shear of velocities was also significant at low water at Sta. 4. The results indicate that complicated current structures are induced at the entrance of the strait when tidal currents flow out from the narrowest part. At the station farthest from the strait and shallowest (Sta. 1), velocities decreased toward the bottom. At the other stations, in contrast, velocities did not always decrease toward the bottom and sometimes velocities in the lower layer were higher than those in the upper layer.

In order to compare the magnitude of tidal currents between ebb and flood tides at the bottom of each station, temporal variations in velocities (m s^{-1}) in the surface and bottom layers are shown in Fig. 7. Bottom velocities are higher during the flood than the ebb tide at all of the stations. Surface velocities are higher during the flood than the ebb tide at Stas. 1 ~ 2, while they are larger during the ebb than the flood tide at Stas. 3 ~ 4. The maximum ebb tides are found about 2 hours before low tide, while the maximum flood tides are found about 3 hours before high tide.

Fig. 8 shows semi-diurnal variations in the squared velocity shear (s^{-2}) calculated using the results from ADCP observation, and turbulent energy dissipation ($\log_{10} \varepsilon$ W m^{-3}) measured using TurboMAP. At all stations, velocity shear near bottom was slightly higher during the flood tide than the ebb. There was a correlation between the variations in turbulent energy dissipation near the bottom and those in velocity shear, in that turbulent energy dissipation increased with velocity shear. At the shallowest station (Sta. 1), velocity shear and turbulent energy dissipation were generally greater than the values at the other stations, reaching near to the surface during flood tide.

At Stas. 2 ~ 4, significant turbulent energy dissipation was found not only near the bottom but also in the middle layer around low water. At Stas. 2 ~ 3, significant velocity shear was found only near bottom, so the energy dissipation found in the middle layer at these stations correlated poorly with velocity shear. At Sta. 4, significant velocity shear and turbulent energy dissipation were observed in the middle layer around low water. The peak dissipation rate at Stas. 2 ~ 3 and Sta. 4 reached ~3×10^{-3} W m^{-3} and 10^{-1} W m^{-3}, respectively.

Vertical profiles of the eastward component of velocity measured using ADCP (m s^{-1}), and shear (s^{-1}) and salinity (psu) measured using TurboMAP are shown in order to examine the variation in turbulent energy dissipation at Sta. 4 (Fig. 9). Note that shear shown in Fig. 9 is obtained from the microstructure profiler, which is different from the vertical shear shown in Fig. 8. At high water the shear signal showed variations with peak value of 0.02 s^{-1}, corresponding to a turbulent energy dissipation rate of 10^{-4} W m^{-3}. During the ebb the shear increased, reaching 0.2 s^{-1}, while the corresponding turbulent dissipation rate was ~ 10^{-1} W m^{-3}.

At high water, salinity profiles showed a vertical difference of 0.2 between the surface and the bottom, and only one halocline was identified around 60 m. During the ebb the salinity profile showed a fine structure with many overturns. At the same time, the vertical salinity difference between the surface and the bottom began to decline. At low water salinity above 80 m was homogeneous, while high-salinity water was found in the layer below 80 m. The profile after low water was completely linear, and vertically averaged salinity was lower than at high water.

5. Discussion

During the observation period wind speed was around 1.5 m s^{-1} and hourly changes in wind speed were insignificant. The profiles and distribution of water density indicated that the influence of wind stirring was confined within the layer above ~ 2 m. There was no evidence of the influence of wind stirring on relatively uniform dissipation through the water column (~ 110 m) observed in this study. The variation in turbulent energy dissipation described in the following is in the absence of wind stirring.

Several studies (e.g. Simpson et al., 1996) showed a predominantly quarter-diurnal variation in turbulent energy dissipation which was strongest near the bed, suggesting significant turbulence originating from the bottom boundary layer twice per semi-diurnal cycle. The variations in turbulent energy dissipation observed in this study, by contrast, were not at quarter-diurnal but at semi-diurnal frequency; turbulent energy dissipation was enhanced during the ebb tide, although it was moderate during the flood.

The asymmetry of turbulent energy dissipation during the ebb and flood tide has been shown by Souza et al. (2008) in the presence of a significant horizontal density gradient. They suggested that Straining Induced Periodic Stratification (SIPS; Simpson et al, 1990) would induce a quarter-diurnal variation in turbulent energy dissipation; turbulence is suppressed by the periodic stratification, while it is enhanced by the reverse differential advection of the stratified water. In our results, by contrast, major asymmetry in turbulent energy dissipation was found in the middle and bottom layers, although density gradients were only formed in the surface layer. The semi-diurnal variation in turbulent energy dissipation might be induced by the other processes.

The higher turbulent energy dissipation near the bottom at all stations during the flood tide is consistent with the greater tidal currents in the bottom layer (Fig. 7). It is suggested that the variations in turbulent energy dissipation near the bottom are strongly influenced by variations in the magnitude of tidal currents in the bottom layer. The tendency for the turbulent energy dissipation in the middle layers of Stas. 3 ~ 4 to be higher during the ebb than during the flood tide is also partly consistent with greater tidal currents and the associated vertical shear of velocities (Fig. 7, Fig. 8).

The maximum turbulent energy dissipation observed throughout the water column at Stas. 2 ~ 4 around low water, after velocities have decreased, however, can not be explained only in terms of the variation in the magnitude of the tidal currents. There is no evidence of an influence of turbulence originating from the bottom boundary layer on the observed, relatively uniform dissipation throughout the water column at these stations. Similar structures have been shown in the shear profiles observed in the studies of Yamazaki et al. (2006) and Mitchell et al. (2008) in Neko Seto.

Tidal currents in the study region flow out from the narrowest part during the ebb and flow in during the flood tide. Significant turbulent energy dissipation was observed at the station nearest the strait (Sta. 4) when tidal currents flow out from the narrowest part (Fig. 8). The velocity shear calculated using ADCP results was significant at low tide. Enhanced turbulent energy dissipation throughout the water column was also observed at Stas. 2 and 3 around low tide, although the velocity shear calculated using results from ADCP was insignificant at Stas. 2 and 3 at that time. Time lags in the maximum dissipation in the middle layer were found between these stations (Stas. 2, 3 and 4). The time lags and the imbalance of the production and dissipation of turbulent kinetic energy implies that turbulent water generated in the strait may be transported and influence the properties of water at these stations located outside the strait when tidal currents flow out from the narrowest part.

Takasugi (1993) showed the temporal variation of tidal energy loss in the strait using control volume analysis (Fig. 2; details of the analysis are shown in the Appendix). Irregularity of tidal currents is generally clearer when they flow out from the narrowest part than when they flow in (Takasugi, 1987). It has been suggested that the variation of the irregularity of tidal currents may possibly have caused the asymmetry of the energy loss in the strait. The present study has established the asymmetry of turbulent energy dissipation in the middle layer of the stations outside the strait. The asymmetry of turbulent energy dissipation outside the strait is largely controlled by the direction of tidal currents and consequently varies at semi-diurnal frequency.

The vertical profiles of temperature and salinity at the station nearest to the strait (Sta. 4) showed the process by which turbulent mixing produces an irreversible conversion of water. Although the vertical differences were identified at high water, the profiles showed step-like structures during the ebb tide, with numerous thermal and saline inversions appearing thereafter. In the middle of the ebb tide the shear was most significant and the turbulent energy dissipation rate exceeded ~ 10^{-2} W m^{-3}. The vertical differences diminished completely after this strong turbulent mixing was observed. Turbulent mixing thus plays an important role in forming a completely mixed water column around the strait.

6. Conclusion

This study has found a semi-diurnal variation in turbulent energy dissipation using a microstructure profiler at the entrance of a tidally energetic strait in the Seto Inland Sea. The results show evidence of significant energy dissipation throughout the water column at the entrance of the strait. They also demonstrate the asymmetry of turbulent energy dissipation in a semi-diurnal tidal cycle, which has been shown by control volume analysis (Takasugi, 1993).

Acknowledgements

Tidal constituents in the study area were provided by the Maritime Safety Agency. The observations were financially supported by the National Institute of Advanced Industrial Science and Technology (AIST Chugoku) and by the Nippon Foundation. The authors wish to express their sincerest appreciation for this support.

References

Inall, M., F. Cottier, C. Griffiths and T. Rippeth (2004): Sill dynamics and energy transformation in a jet fjord. Ocean Dynamics, 54, 307-314.

Kobayashi, S., J. H. Simpson, T. Fujiwara and K. J. Horsburgh (2006): Tidal stirring and its impact on water column stability and property distributions in a semi-enclosed shelf sea (Seto Inland Sea, Japan). Cont. Shelf Res., 26, 1295-1306.

Matsuno, K. and H. Nakata (2004): Physical Processes in the Current Fields of Ariake Bay. Bulletin on Coastal Oceanography, 42, 11-17.

Mitchell, J. G., H. Yamazaki, L. Seuront, F. Wolk, and H. Li (2008): Phytoplankton patch patterns: Seascape anatomy in a turbulent ocean. J. Marine Systems, 69, 247-253.

Nasmyth, P. W. (1970): Ocean turbulence. Ph. D. Thesis, Univ. Of British Columbia, Vancouver, Canada, 69 pp.

Oakey, N. S. and J. A. Elliott (1980): The Variability of temperature- gradient microstructure observed in the Denmark Strait. J. Geophys. Res.-Oceans, 85, 1933-1944.

Oakey, N. S. (1982): Determination of the rate of dissipation of turbulent energy from simultaneous temperature and velocity shear microstructure measurements. J. Phys. Oceanogr.,12, 256-271.

Peters, H. (1999): Spatial and temporal variability of turbulent mixing in an estuary. J. Marine Research, 57, 805-845.

Simpson, J. H., J. Brown, J. Matthews and G. Allen (1990): Tidal Straining, density currents, and stirring in the control of estuarine stratification. Estuaries, 13, 125-132.

Simpson, J. H., H. Burchard, N. R. Fisher and T. P. Rippeth (2002): The semi-diurnal cycle of dissipation in a ROFI: model-measurement comparisons. Cont. Shelf Res., 22, 1615-1628.

Simpson, J. H., W. R. Crawford, T. P. Rippeth, A. R. Campbell and J. V. S. Cheok (1996): The Vertical Structure of Turbulent Dissipation in Shelf Seas. Journal of Physical Oceanography, 26, 1579-1590.

Souza, A. J., N. R. Fisher, J. H. Simpson and M. J. Howarth (2008): Effects of tidal straining on the semidiurnal cycle of dissipation in the Rhine region of freshwater influence: Comparison of model and measurements. J. Geophys. Res.-Oceans, 113, C01011.

Takasugi, Y. (1993): Fine structures of the tidal current in and around the straits and their functions in sediment transport. Reports of Chugoku National Industrial Research Institute, 11, 127 pp.

Takasugi, Y. (1987): Characteristics of velocity distributions in a strait: current measurements by Doppler Current Profiler. La mer, 25,167-174.

Takasugi, Y. (1989): Formation of sand banks due to tidal vortices around strait. J. Oceanography, 50, 81-98.

Takeoka, H. (2002): Progress in Seto Inland Sea Research. J. Oceanography, 58, 93-108.

Wolk, L. and R. G., A. Lueck (2002): New Free-Fall Profiler for Measuring Biophysical Microstructure. J. Atmospheric and Oceanic Technology, 19, 780-793.

Yamazaki, H., J. G. Mitchell, L. Seuront, F. Wolk and H. Li (2006): Phytoplankton microstructure in fully developed oceanic turbulence. Geophysical Res. Lett.,33, L01603.

Figure Captions

Fig. 1.

(a) Location of the Seto Inland Sea. (b) Location of Neko Seto, one of the straits in the Seto Inland Sea. The study area covers the entrance of Neko Seto. Circle indicates the position where harmonic constants were obtained by the Maritime Safety Agency. (c) Bathymetry of the Neko Seto. Cntours indicate water depth in meters (contour interval = 10 m). Stations indicated by circles (C1 ~C6) and dotted lines marked ‘A’ and ‘B’ were used in Takasugi (1993).

Fig. 2.

Temporal variations in terms of equation of tidal energy balance applied to the study area (after Takasugi, 1993). E_t, E_k, E_p, and E_f indicate time rate of change of kinetic energy, divergence of kinetic energy flux, divergence of potential energy flux, and energy loss, respectively. E_w and W_w indicate the direction of tidal flows, eastward and westward, respectively.

Fig. 3.

Map of the study area. Black circles indicate observation points (stations 1 ~ 4). Numbers in parentheses denote water depths at these points. Arrows show the directions of flood and ebb tide in the study area.

Fig. 4.

Temporal variations of tidal height (m) at the point located at the western end of the study area (see Fig. 1b) on 6 July 2005, predicted using tidal constituents (M_2, S_2, K_1, O_1) provided by the Maritime Safety Agency, Japan.

Fig. 5.

Distributions of (a) temperature (deg C), (b) salinity (psu) and (c) sigma-t in the upper layer (0 ~ 40 m) in the axial sections observed at 09:45 h (high water) (a ~c), 13:00 h (ebb tide) (d ~ f), 15:20 h (low water) (g ~ i) and 18:30 h (flood tide) (j ~ l) on 6 July 2005; all times in JST. Contour intervals are 0.1. Ticks above each figure indicate observation points. Station locations are shown in Fig. 3.

Fig. 6.

(a, c, e, g) Temporal variations in eastward components of velocities (m s^{-1}) measured using ADCP on 6 July 2005 at stations 1 ~ 4. Positive and negative values are eastward and westward, respectively. (b, d, f, h) Temporal variations in northward components of velocities (m s^{-1}). Positive and negative values are northward and southward, respectively. Velocity data taken at 2 m intervals are vertically interpolated to make a 1 m interval dataset. Color bars are shown on the right side of the panels. Contour intervals are 0.05 (m s^{-1}). Broken lines in each figure indicate water depths at the stations. Ticks above each figure indicate the time of measurement. Data between measurements are obtained by linear interpolation.

Fig.7.

Temporal variation in velocities (m s^{-1}) measured using ADCP on 6 July 2005 at (a) Sta.1, (b) Sta.2, (c) Sta.3 and (d) Sta.4. Thin lines with open squares and thick lines with closed squares show the velocities in the surface and bottom layers, respectively. Surface layers are set to 5 m at all stations, while the bottom layers are set to 11 m, 25 m, 51 m and 103 m at Sta. 1, 2, 3 and 4, respectively.

Fig. 8.

(a, c, e, g) Temporal variation in squared velocity shear (s^{-2}) calculated using the results from ADCP shown in Fig. 6. Color bar is shown on the upper right side of the panels. Contour intervals are 0.002 (s^{-2}). (b, d, f, h) Temporal variation in turbulent energy dissipation ($\log_{10} \varepsilon$ W m^{-3}) measured using TurboMAP on 6 July 2005 at stations 1 ~ 4. Color bar is shown on the lower right side of the panels. Contour intervals are 0.5. Broken lines in each figure indicate water depths at the stations. Ticks above each figure indicate the time of measurement.

Fig. 9.

Vertical profiles of the eastward component of velocity measured using ADCP (m s^{-1}), and shear (s^{-1}) and salinity (psu) measured using TurboMAP at station 4 at (a) 10:10 h (high water), (b) 13:20 h (ebb tide), (c) 15:45 h (low water), and (d) 16:30 h (flood tide) on 6 July 2005.

Appendix

Analysis of tidal energy balance in Neko Seto (Takasugi, 1993)

Tidal energy balance in the study area was investigated by Takasugi (1993), on the basis of the results of the continuous observations conducted in 1988. In the observations, pressure sensors were set up at four points around the strait to measure hourly sea level. Two ships mounted ADCP ran for 25 hours from 14 - 15 September 1988 to measure the current velocities along the two sections labeled 'A' and 'B' in Fig. 1c.

Based on these data, tidal energy balance between sections A and B was estimated. Assuming the currents in the strait can be treated as one-dimensional flow, the balance of energy is represented as:

$$\frac{\partial}{\partial t}\left[\int_S \frac{1}{2}\rho u^2 dS\right] + \frac{\partial}{\partial x}\left[\int_S \frac{1}{2}\rho u^3 dS\right] + \rho g Q \frac{\partial h}{\partial x} = -E_f \quad ,$$

where ρ is the density, g is the gravitational acceleration, h is the water depth, t is time, x is the distance along the strait, u is the velocity orthogonal to the sections and $S(=5\times10^4\,\mathrm{m}^2)$ is the average area of the sections. Q is the volume flux through the section, which is represented as $Q=\overline{U}S$, where $\overline{U}=\int_S udS/S$ is the sectional averaged velocities. The first term (E_t) indicates time rate of change of kinetic energy, the second (E_k) is divergence of kinetic energy flux, the third (E_p) is divergence of potential energy flux, and fourth (E_f) is energy loss which is caused by bottom, wall and internal frictions in water column. E_t and E_k are obtained from integration of the observed cross-sectional velocity, E_p is obtained from those of sea level at the stations at the entrance of the strait and E_f is derived from these three terms as their residuals.

Fig. 2 shows the temporal variations of each term. E_t and E_k are relatively small or negligible. The energy loss, E_f, reaches 2.5 × 10^4 Wm^{-1} during maximum ebb and flood. It is notable that the magnitude of E_f changes according to the current direction; it became larger in westward than that in eastward flow. Significant horizontal shear has been observed in tidal currents, developed due to the effect of the local geometry when the tidal current is toward the west. This result indicates that internal friction in the water column significantly influences the energy loss around the strait, as does bottom friction.

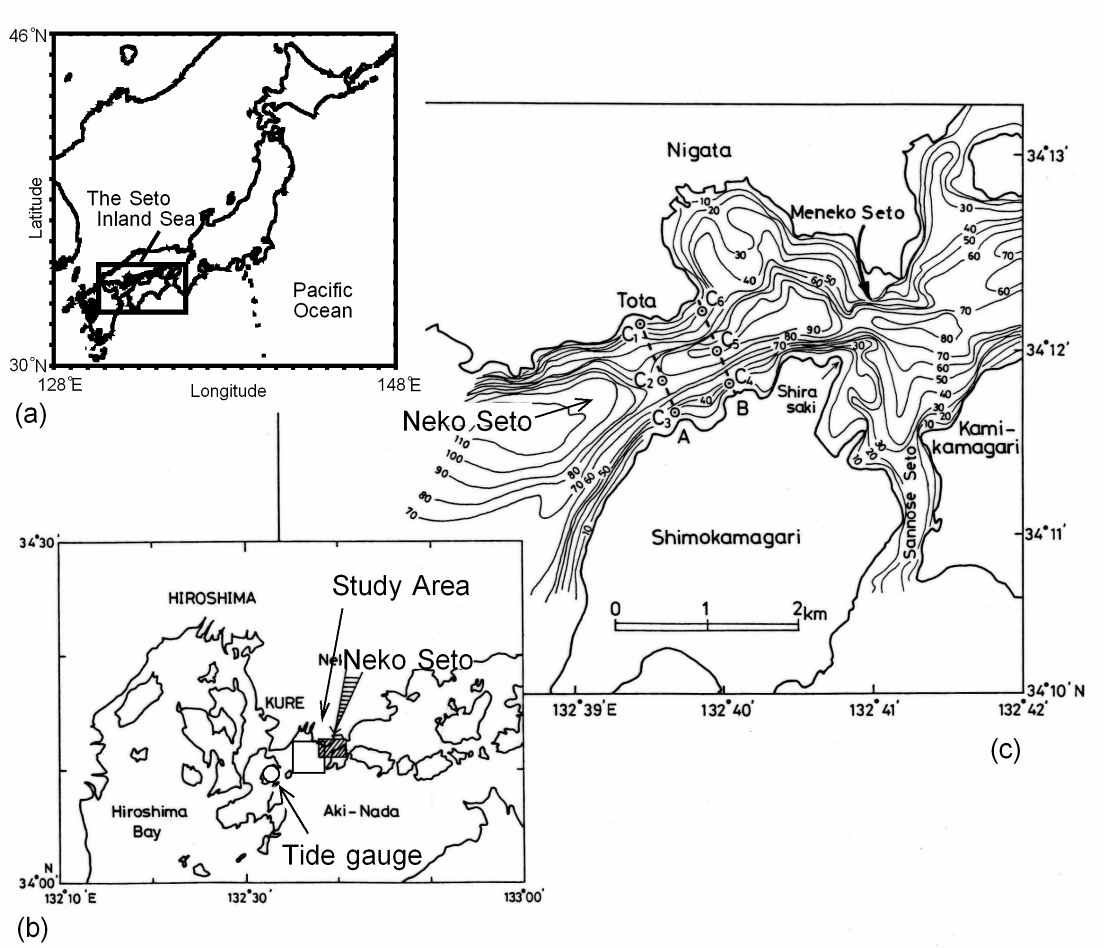

Fig. 1 (Kobayashi et al)

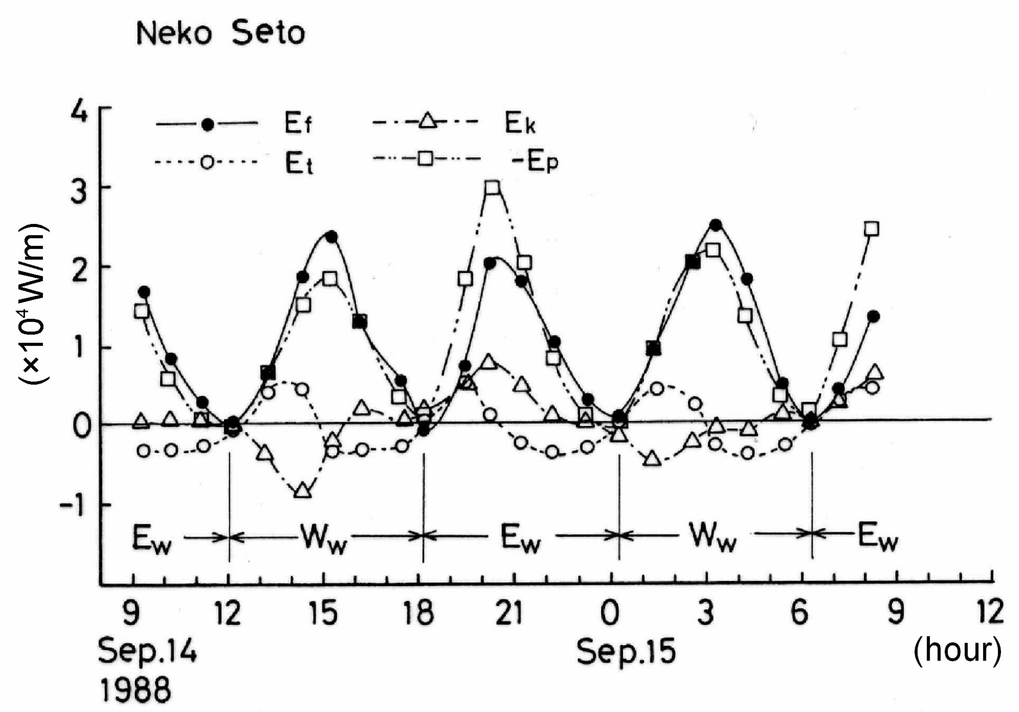

Fig. 2 (Kobayashi et al)

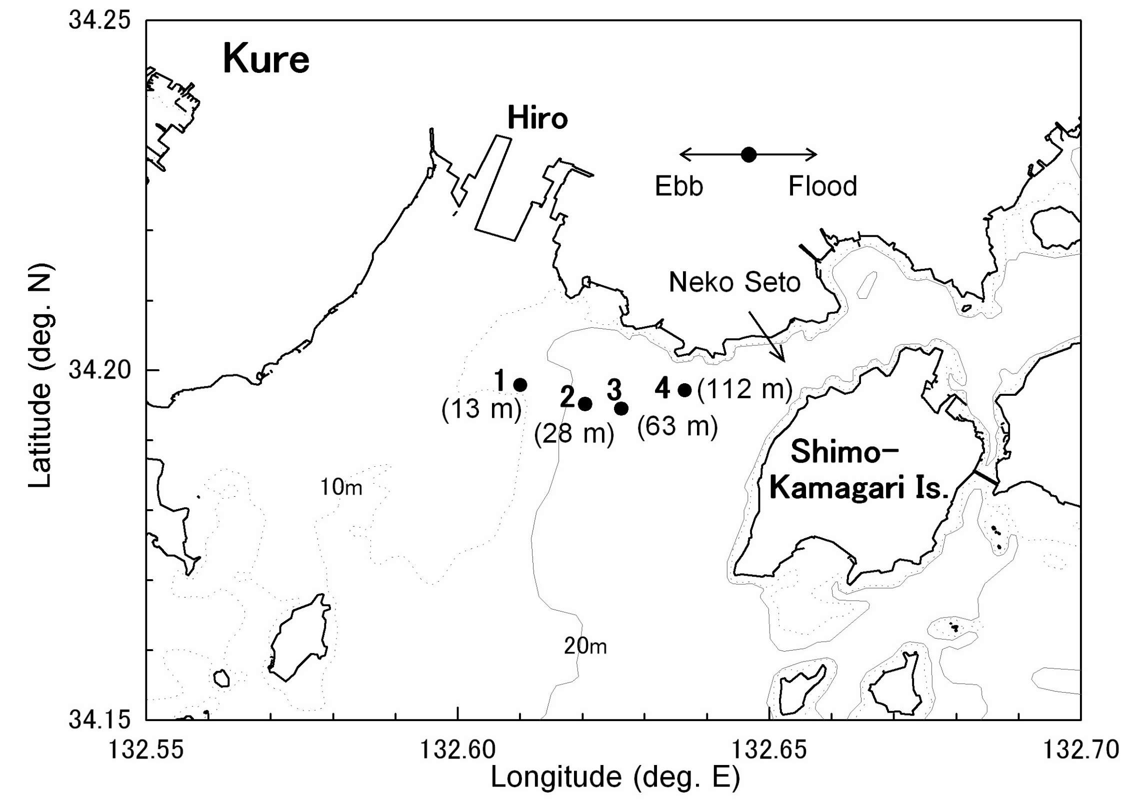

Fig. 3 (Kobayashi et al).

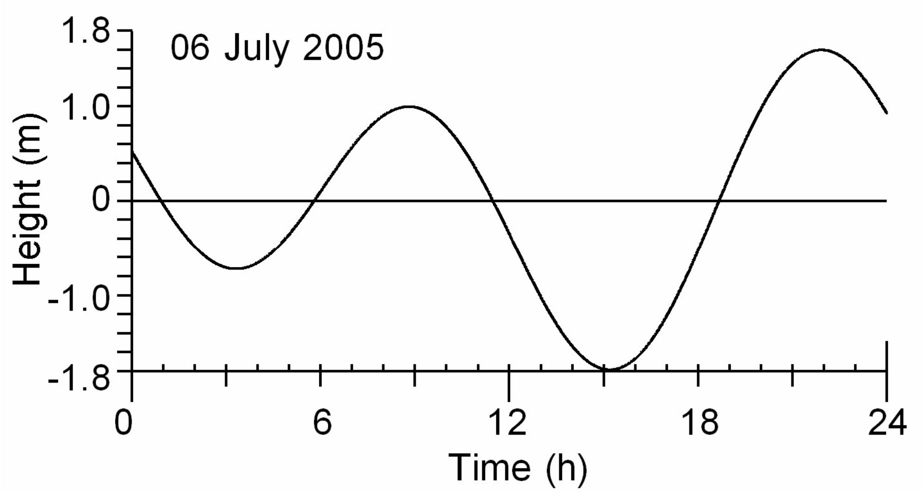

Fig. 4 (Kobayashi et al).

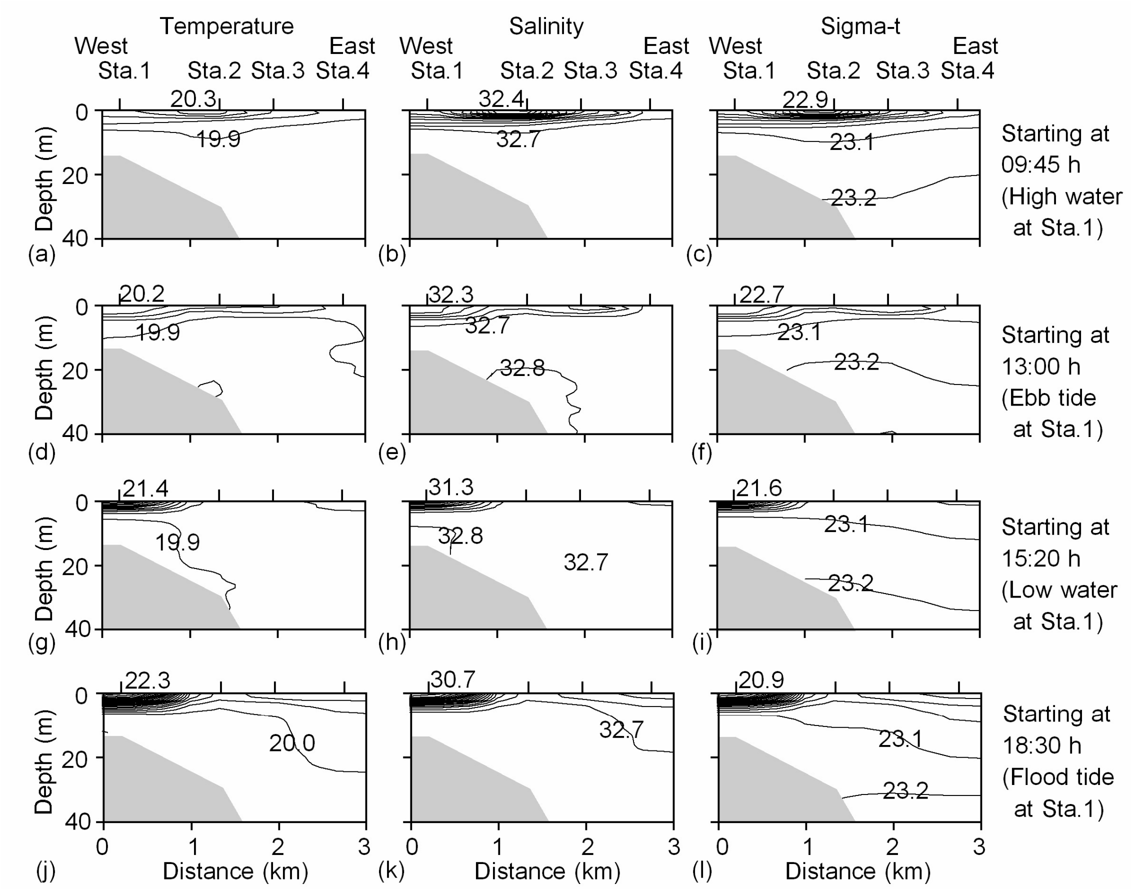

Fig. 5 (Kobayashi et al)

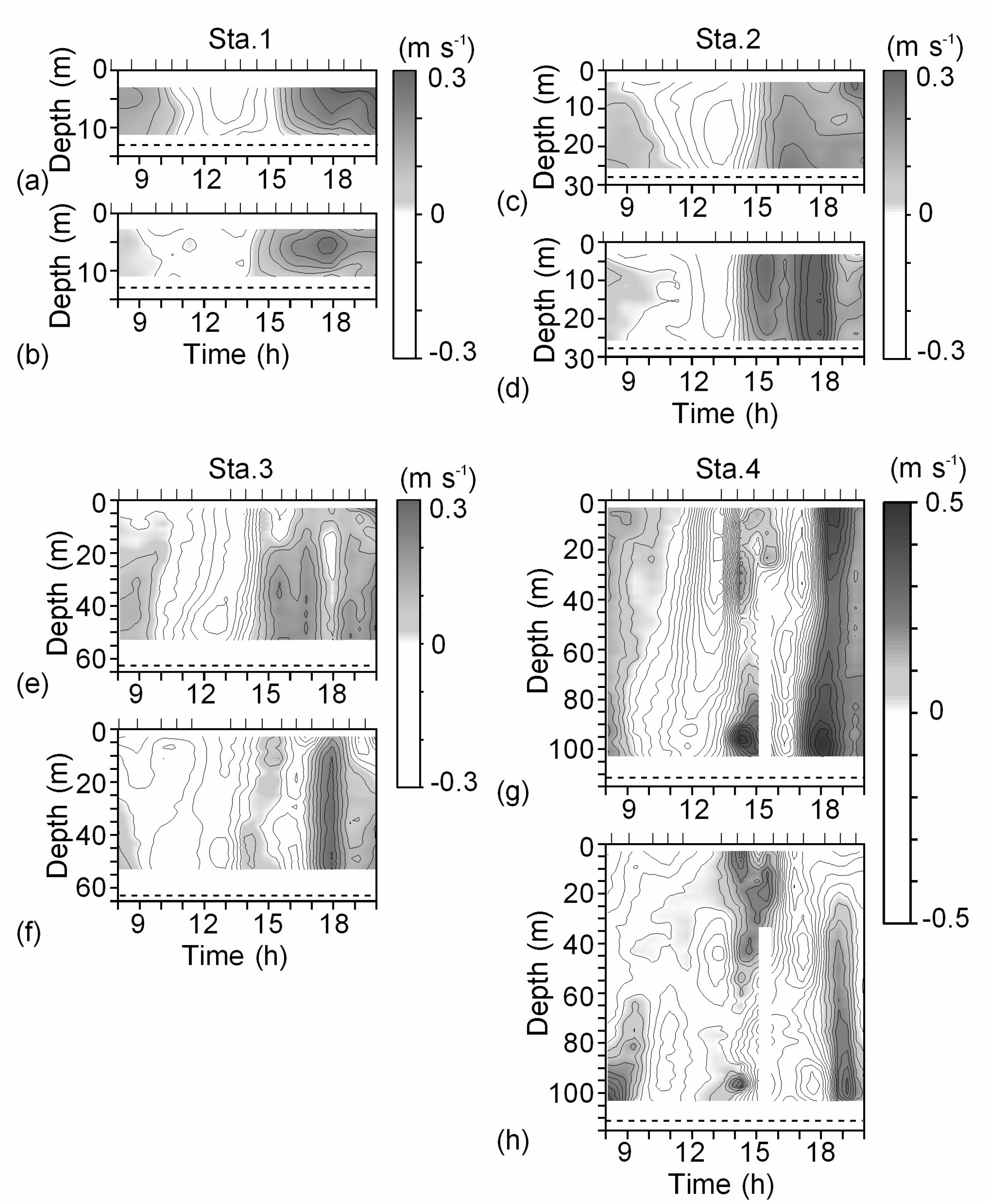

Fig. 6 (Kobayashi et al)

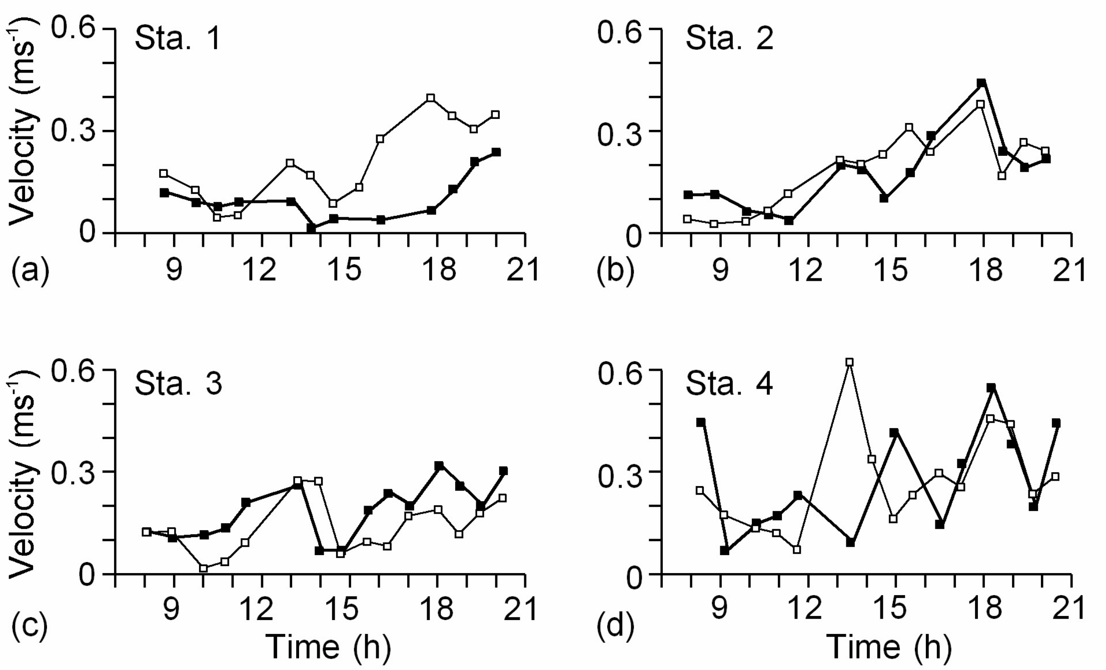

Fig. 7 (Kobayashi et al)

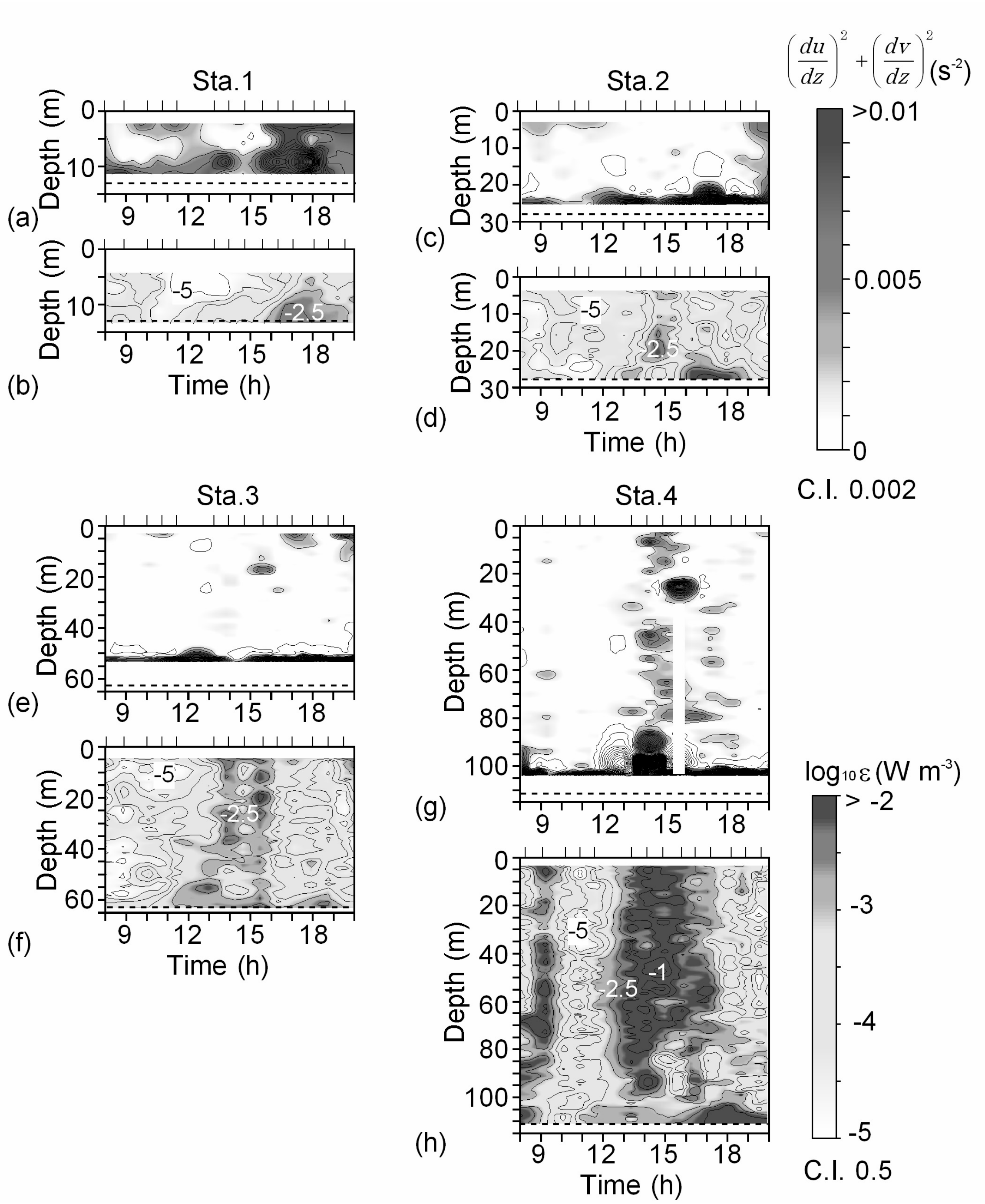

Fig. 8 (Kobayashi et al)

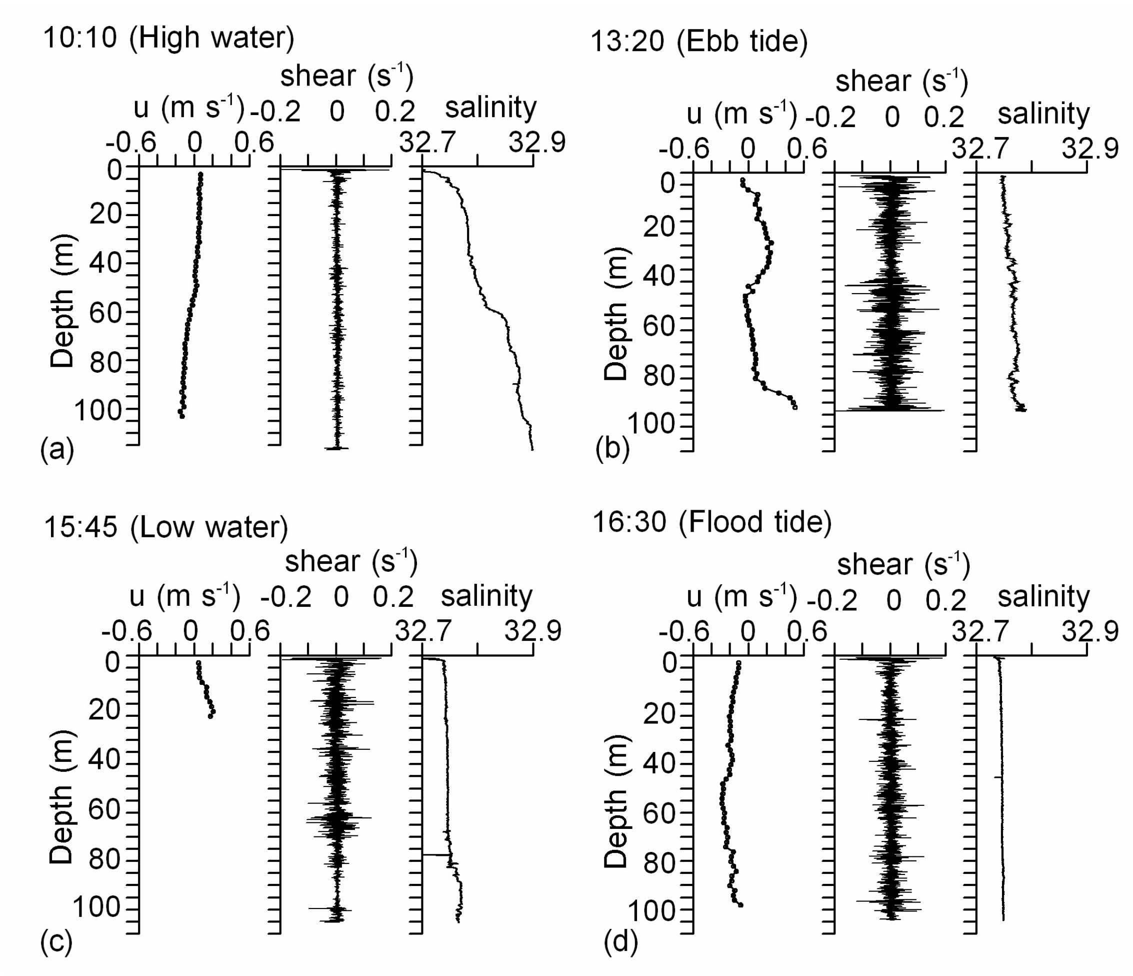

Fig. 9 (Kobayashi et al)